CrossMark

ORIGINAL PAPER

Green method to reinforce natural rubber with tunicate cellulose nanocrystals via one-pot reaction

Liming Cao · Daosheng Yuan · Xingfeng Fu · Yukun Chen

Abstract Tunicate cellulose nanocrystals (t-CNs) isolated from marine biomass were mixed with natural rubber (NR) via two different approaches. The first approach was the green one-pot route, NR latex was first mixed with t-CNs suspension, followed by epoxidization of the mixture. Meanwhile, a two-step method, referring to the way that NR latex was first epoxidized and then mixed with t-CNs suspension, was also carried out for comparison. The interfacial interaction, thermal performance, morphology, mechanical properties and water swelling behavior were investigated. Hydrogen bonds formed in the both nanocomposites and mechanical properties improved with increasing t-CNs content. Moreover, better dispersion and enhanced interfacial interaction were achieved for one-pot method, which was ascribed to the etching effect of hydrogen peroxide on the t-CNs surface and the possible grafting reaction during one-pot process. Therefore, compared with two-step method, 20% increase in tensile strength and 50% increase in tensile modulus were achieved for one-pot method at 10 phr t-CNs content.

L. Cao · D. Yuan · X. Fu · Y. Chen (✉)
Lab of Advanced Elastomer, South China University of Technology, Guangzhou 510640, China
e-mail: cyk@scut.edu.cn

Introduction

Substantial attention has been paid to biobased materials because of their potential for producing a variety of high-value products without deteriorating the environment. Cellulose nanocrystals (CNs) are highly crystalline rod-like nanomaterials that can be isolated from various biosources, such as plants (e.g., cotton, wood, or straw, etc.), marine animals (tunicate), and bacterial sources as well (Sacui et al. 2014; Lin et al. 2012; Moon et al. 2011). The abundant availability, environmental friendliness and superior mechanical properties of CNs make them a desirable reinforcing phase for polymer nanocomposites. The investigation of using CNs as reinforcing filler in polymer matrice was first reported by Favier et al. in 1995 (Favier et al. 1995). Since then, the interest in exploring CNs as reinforcing phase in polymer nanocomposites has grown tremendously, involving a broad range of CNs isolated from various resources as well as different kinds of polymer matrices such as poly(vinyl alcohol), polyurethane, polyethylene oxide, polylactic acid and natural rubber, etc. (Song et al. 2016; Saralegi et al. 2014; Ye et al. 2016; Pei

et al. 2011; Tian et al. 2016; Liu et al. 2017; Spinella et al. 2015; Scafaro et al. 2017).

However, the critical challenge to achieve effetient transfer from exceptional properties of CNs to macroscale properties of the bulk nanocomposites depends on the ability to obtain well-dispersed CNs in polymer matrices. Yet the interfacial interaction between CNs and polymer matrices is another challenge should be addressed (Chen et al. 2016, 2017; Xu et al. 2018). Therefore, the development of exploring nanocomposites with homogeneously dispersed CNs and strong interfacial adhesion is a critical and indispensable aim. Great efforts have been made to obtain satisfactory dispersion of CNs in polymer matrices, involving melt blending, solution mixing, latex technology, and in situ polymerization, etc. (Lin and Dufresne 2013; Fortunati et al. 2015; Cao et al. 2009; Oksman et al. 2016). Among them, solution mixing has been demonstrated to be an effective method to obtain satisfactory dispersion, but the removal of large amount of solvent limits its wide application (Fortunati et al. 2015; Cao et al. 2009; Fu et al. 2018). Melt mixing is highly pursued due to the industrial availability. However, it always exhibits poor dispersion of CNs and may lead to degradation of CNs during melt compounding (Bitinis et al. 2013). Latex co-coagulation technology is a very simple and efficient method to yield homogeneous dispersion of nanofillers in polymer matrices because the aggregation of nanoparticles could be kinetically prevented by the faster coagulation of the latex particles. It has been successfully applied for preparing well-dispersed graphene oxide, carbon nanotubes or clay-based polymer nanocomposites (Tang et al. 2012; George et al. 2017; Ha et al. 2008).

To satisfy the growing interest of improving the performance of composites using CNs, the interfacial interaction between CNs and polymers should be taken seriously. Owing to the abundant hydroxyl groups on CNs surface, hydrogen bonds is considered as an effective way to improve interfacial interaction between CNs and matrix (Cao et al. 2013; Chen et al. 2015; Mariano et al. 2016). Nevertheless, hydrogen bonds are not strong enough to prevent aggregation of CNs and transfer load from matrix to CNs under external stress efficiently, which yields moderately improved performance. Surface chemistry, including surface-initiated polymerization (Miao and Haman 2016), covalent functionalization (Kanoth et al. 2015),

and the use of surfactants (Bitinis et al. 2013), etc., is another strategy to improve interfacial interaction between CNs and polymers. For example, Yu et al. (Yu et al. 2016) designed functionalized CNs via surface-initiated atom transfer radical polymerization (ATRP), and these functionalities could serve as anchoring sites and open the way to further derivative reactions that enhanced compatibility between matrix and CNs. Utilizing the esterification reaction between CNs and matrix, CNs could serve as not only reinforcing phase, but also crosslinking agent, and thus produced nanocomposites with unique mechanical behavior (Goetz et al. 2010). Although these approaches are envisaged as efficient strategies to improve the dispersion of CNs and interfacial interaction between CNs and matrices, they involved with large amounts of organic solvents and the use of expensive deliberately made chemicals, which greatly limit their wide application. Thus, exploring simple and efficient approaches to improve interfacial interaction in polymer/CNs nanocomposites is of great importance.

Natural rubber (NR) is a biobased and biocompatible polymer with numerous carbon–carbon double bond on its backbone (Xu et al. 2016, 2017; Chen et al. 2018), which enables the chemical modifications of NR. Especially the epoxidization, which produces epoxidized natural rubber (ENR) with randomly distributed epoxy groups along with the backbone via hydrogen peroxide (H_2O_2) (Yu et al. 2008). At the same time, starch which has similar chemical structure with CNs, could also be oxidized by H_2O_2 under weak acid conditions (Zhang et al. 2015). Inspired by these study, herein, we prepared biobased rubber nanocomposites with tunicate CNs (t-CNs) via two different approaches, as illustrated in Scheme 1. Namely, green one-pot approach, NR latex was mixed with t-CNs suspension firstly, and then the mixture were further epoxidized. Meanwhile, two-step approach, in which NR latex was epoxidized firstly and then mixed with t-CNs suspension was also carried out as comparison. The morphology, mechanical properties and water swelling behavior of the nanocomposites were studied and compared in detail.
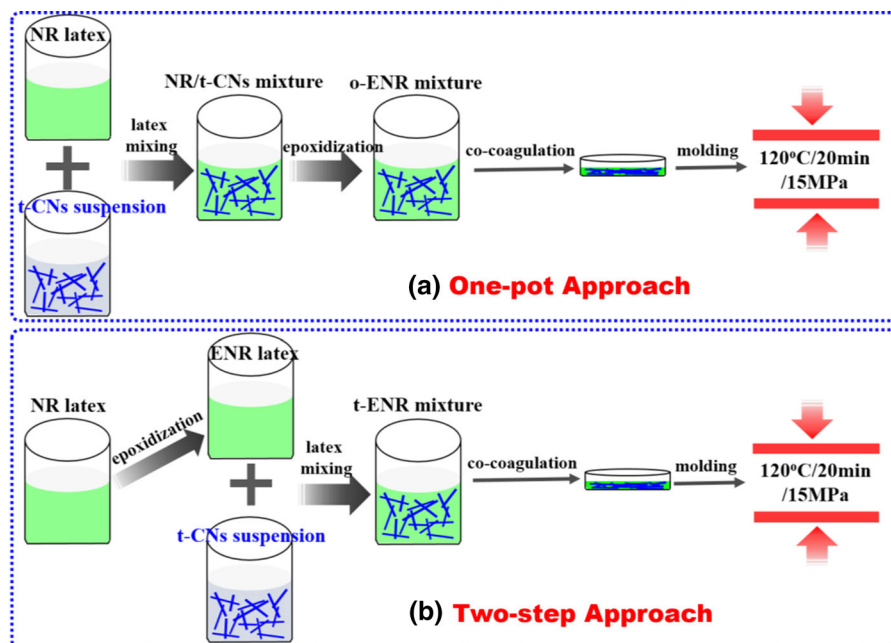
Scheme 1 Illustration of processing of **a** one-pot approach: NR latex was mixed with t-CNs suspension firstly, and then the mixture were further epoxidized; **b** two-step approach: NR latex was first epoxidized, and then mixed with t-CNs suspension

Experimental

Materials

Natural rubber latex with 60 wt% solid content was kindly supplied by Agricultural Products Processing Research Institute (Zhanjiang, China). All reagents, solvents and other chemicals were analytically pure and used as received without further purification. Tunicate cellulose nanocrystals (t-CNs) were isolated form mantles of sea animal termed tunicate (*Halocynthia roretzi*), via sulfuric acid hydrolysis according to procedure reported previously (see Supporting Information) (Cao et al. 2017a, b). Multiple batches of t-CNs obtained via this protocol were used, which showed similar morphology and structure.

Fabrication of ENR/t-CNs nanocomposites via green one-pot approach (o-ENR system)

Green one-pot route was used to fabricate ENR/t-CNs nanocomposites. In the typical experiment, premeasured quantities of t-CNs suspension were subsequently added to NR latex firstly, and the mixtures were ultrasonicated under 100 W for 30 min with frequency of 40 kHz. Then epoxation reaction were

carried out (see Supporting Information for detailed procedure). After epoxidization reaction, the resulting mixtures were co-coagulated by adding alcohol and washed with deionized water several times to remove excess alcohol. The compounds were vacuum dried at 50 °C over night. Then the dried compounds were further compression molded at 120 °C for 20 min, using spacers to control the thickness, and subsequently cooled down to room temperature to yield 500 ± 90 μm thick specimens. Pressing conditions were optimized to obtain nonshrinking, free-standing specimens. These "one-pot" nanocomposites are coded as "o-ENR-x", where "x" represents the parts per hundred of rubber (phr) of t-CNs in the nanocomposites.

Fabrication of ENR/t-CNs nanocomposites via two-step approach (t-ENR system)

For comparison, two-step method was also conducated. NR was first epoxidized to introduce randomly distributed epoxy groups according to previous study (Yu et al. 2008). The detailed procedure is illustrated in Supporting Information. Then t-ENR nanocomposites were prepared by mixing appropriate ratios of the two suspensions and then ultrasonicated under 100 W

for 30 min with frequency of 40 kHz. Following procedures after ultrasonication were the same with the preparation of o-ENR nanocomposites. The codes for nanocomposites prepared via two-step approach are "t-ENR-x", where "x" represents the parts per hundred of rubber (phr) of t-CNs in the nanocomposites.

Characterizations

Fourier transform infrared spectroscopy (FTIR) was conducted on a Bruker Tensor 27 FTIR Spectrometer. KBr plate method was used in taking IR spectra. Suspension with a certain concentration was dropped on KBr disc (sample/KBr ratio was 1/100) and dried before observation. The experiments were conducted with resolution being 4 cm^{-1} and total of 32 scans. Spectra were collected from 4000 to 600 cm^{-1}.

Dynamic mechanical analysis (DMA) was carried out on the NETZSCH DMA 242 C analyser in tension mode. The tests were conducted at frequency of 1 Hz and strain amplitude of 20 μm in temperature range of − 60 to 50 °C, and with scanning rate of 3 °C/min.

Differential scanning calorimetry (DSC) measurements were conducted under nitrogen atmosphere on the NETZSCH DSC 204 F1 (Germany). Two heating ramps were carried out in temperature range from − 50 to 20 °C with scanning rate of 10 K/min, and glass transition temperatures (T_gs) of the samples were determined from the second heating cycle.

Scanning electron microscopy (SEM) and Transmission electron microscopy (TEM) were used to observe the dispersion state of t-CNs in ENR matrix. For SEM imaging, the specimens were frozen in liquid nitrogen, snapped and then coated with a thin layer of platinum before observation. For TEM observation, specimens were cryo-microtomed at − 80 °C using the Leica EM UC6 equipment. Images were recorded without any prior staining using JEM-2100F operating at 200 kV.

Atomic force microscopy (AFM) was used to observe the morphology of the obtained t-CNs and was carried out using Multimode 8 (Bruker, Germany) instrument operated in tapping mode. A certain concentration of t-CNs suspension were dropped onto freshly cleaved mica surfaces before observation.

Bound rubber content (BRC) of the nanocomposites were calculated according to the following procedure: about 2 g of rubber compound was cut

into pieces and packaged with filter paper, then immersed in chloroform (CHCl$_3$) for 72 h during which the solvent was updated every 24 h. After that, the compound was dried to constant weight in vacuum oven under 50 °C. BRC was calculated according to the equation:

$$BR = \frac{M_0 - (M_1 - M_2)}{M_0} \times 100\% \qquad (1)$$

where M_0 is rubber weight in the sample, M_1 is sample weight including copper net, and M_2 is sample weight including copper net after dried (Liu et al. 2015a, b).

The mechanical properties of the samples were measured on the Universal Materials Testing Machine from UCAN, Taiwan China, equipped with a 1000 N load cell. Tensile tests were performed at 23 °C with gauge length of 20 mm and crosshead speed of 500 mm/min. Five specimens were measured for each sample to get an average value.

The water-swelling behavior of the nanocomposites were conducted in deionized water at ambient condition. The samples were first dried under vacuum at 60 °C for 24 h and weighed with analytical balance. Then they were immersed in deionized water and removed every 24 h, gently blotted with filter paper, weighed, and immersed in deionized water again immediately. Water-swelling behavior were carried out for 4 days and were conducted in triplicate for each sample. The water uptake (W_U) was determined from the equation listed as follow:

$$W_U = \frac{M_t - M_0}{M_0} \times 100\% \qquad (2)$$

where M_0 and M_t are masses of the sample before immersion and immersed for a certain period of time t, respectively.

Results and discussion

Interfacial interaction in t-ENR and o-ENR systems

In this study, t-CNs were isolated from tunicate (*Halocynthia roretzi*) mantles via sulfuric acid hydrolysis method. As a consequence t-CNs surface is decorated with negatively charged sulfate groups, which is beneficial for its stable dispersion in water. Figure 1 shows the AFM image of t-CNs and its

Fig. 1 a AFM images of t-CNs; b transverse height profiles determined
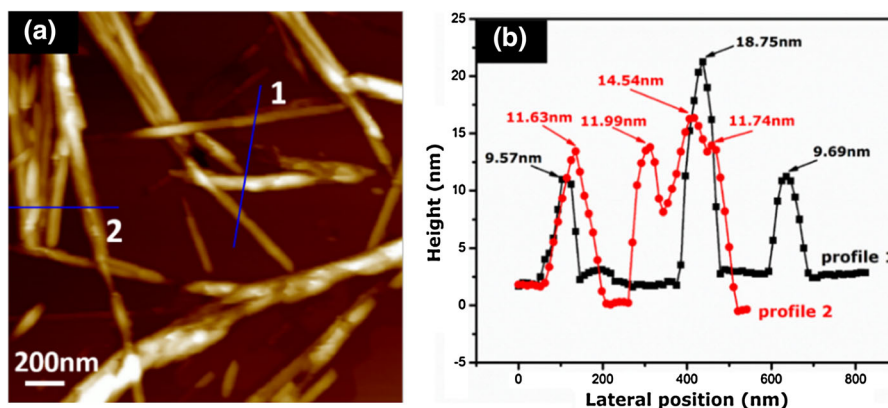
corresponding height profile. It can be seen that these isolated t-CNs have dimensions of 10–20 nm in diameter, 500 nm to 2 μm for length, and with a large aspect ratio of ∼ 75, which is similar to those isolated from tunicate mantles previously reported (Fox et al. 2012; Zhao et al. 2015).

The interaction between two components was investigated by FTIR measurements. As shown in Fig. 2, t-CNs show typical cellulose structure characteristics, with –OH, C–H and C–O stretching vibrations at 3347, 2902 and 1058 cm^{-1}, respectively (Zhao and Li 2014). The peak around 1641 cm^{-1} is associated with –OH bending vibration of absorbed water (Zhao et al. 2015). In the spectra of t-ENR-10 compound, the absorption band corresponding to –OH is shifted to lower wavenumber from 3347 to 3334 cm^{-1}, indicating the formation of hydrogen

bonds between epoxy groups in ENR chains and hydroxyl groups on the surface of t-CNs (Liu et al. 2017; Tang et al. 2012). It is worth noting that this absorption band further shifted to 3321 cm^{-1} for o-ENR-10 compound, indicating stronger interfacial interaction compared with t-ENR-10. The improved interfacial interaction may be caused by (1) the hydrogen bonds interaction and (2) the strong physical absorption, which lead to the formation of more bound rubber in o-ENR-10 compound (Liu et al. 2015a, b; Xu et al. 2015; Wolff et al. 1993). As shown in Fig. 3, BRC increased with increasing t-CNs content, and o-ENR nanocomposites shows even higher BRC than t-ENR nanocomposites, especially with higher t-CNs content. Indicating stronger entanglements between ENR and t-CNs in o-ENR nanocomposites are formed.
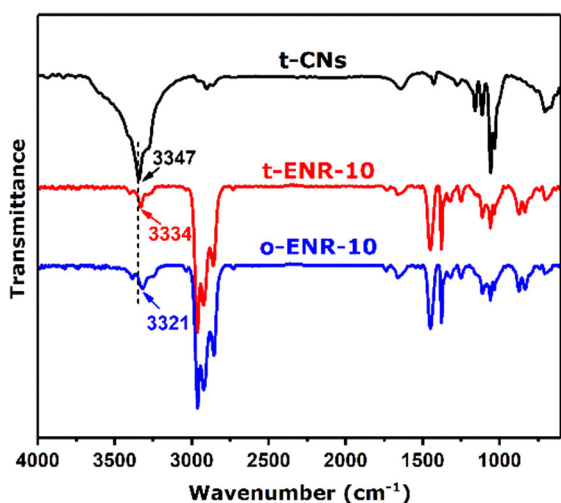

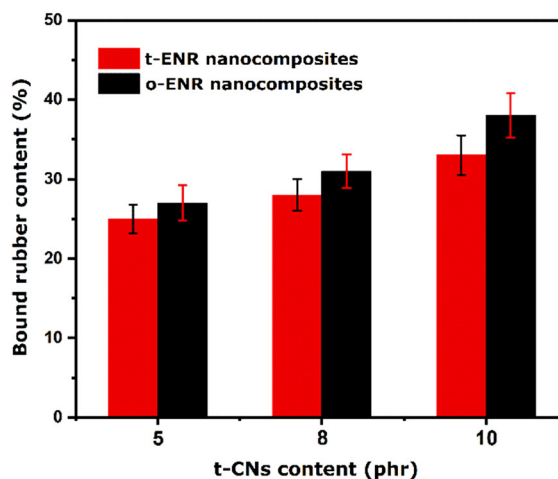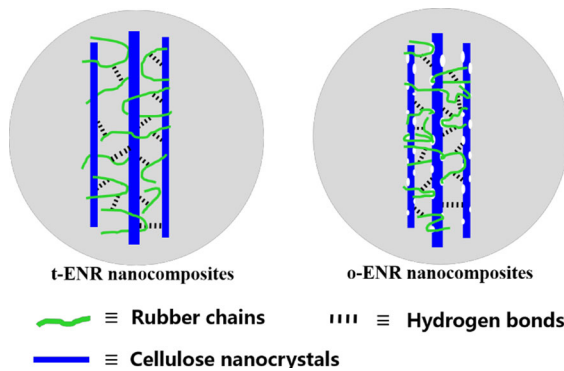Fig. 2 FTIR spectra of t-CNs, t-ENR-10 and o-ENR-10 compounds

Fig. 3 Bound rubber content of ENR/t-CNs nanocomposites with different t-CNs contents
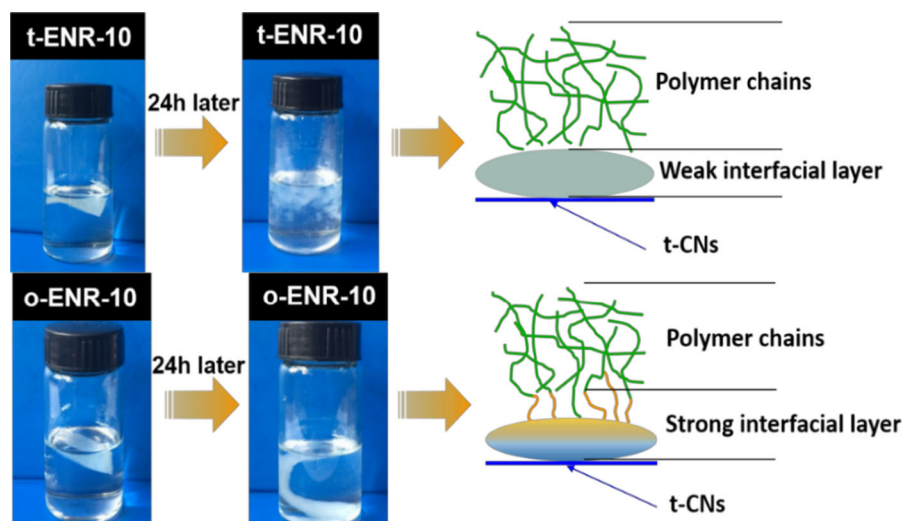
Scheme 2 Illustration of the interfacial interaction between rubber chains and t-CNs in t-ENR and o-ENR nanocomposites

Some erosions will begin to form on the surface of t-CNs due to the strong oxidization of H_2O_2 in the one-pot reaction, which will ultimately result in massive defects. These defects could absorb more rubber chains onto its surface and make them bond together tightly, which is beneficial for the formation of more bound rubber, as depicted in Scheme 2. On the other hand, as indicated previously, both t-CNs and NR could be oxidized or epoxidized in the presence of H_2O_2 under acid conditions (Yu et al. 2008; Cao et al. 2017a, b; Yan et al. 2017). Thus, grafting reaction may also occur between t-CNs and ENR during one-pot process, which could also contribute to the enhanced interfacial interaction in o-ENR system.

In order to further study the interaction between ENR and t-CNs, swelling behavior of the nanocomposites were characterized, as shown in Fig. 4. It can

be seen that after immersed in toluene for 24 h, t-ENR-10 sample is dissolved into small pieces with 5 min ultrasonic treatment under 40 W with frequency of 40 kHz because of the weak interfacial interaction. Comparatively, only swelling behavior is observed for o-ENR-10 sample under the same treatment, indicating the improved interacfical interaction in o-ENR system.

Thermal analysis of ENR/t-CNs nanocomposites

DSC and DMA measurements were conducted to characterize the glass transition temperature (T_g) of neat ENR and resultant nanocomposites. As shown in Fig. 5, T_g increases slightly with increasing t-CNs content in the nanocomposites. The increase in T_g indicates that the polymer chains were indeed constrained by hydrogen bonds. However, it is worth noting that compared with t-ENR system, o-ENR nanocomposites show a little higher T_g at same t-CNs content. The higher $T_g s$ of o-ENR system might be due to (1) the effect of hydrogen bonds interaction and (2) the more bound rubber content, which further restrict the segment motion of ENR chains (Ha et al. 2008; Kanoth et al. 2015). Therefore, the rubber chain segments could move at higher temperatures as discussed above.

Morphology of ENR/t-CNs Nanocomposites

In addition to interfacial interaction, the dispersion of filler in matrix is another important factor that affect

Fig. 4 Photographs of swelling behavior of o-ENR-10 and t-ENR-10 nanocomposites in toluene and proposed model of the interface structure of them
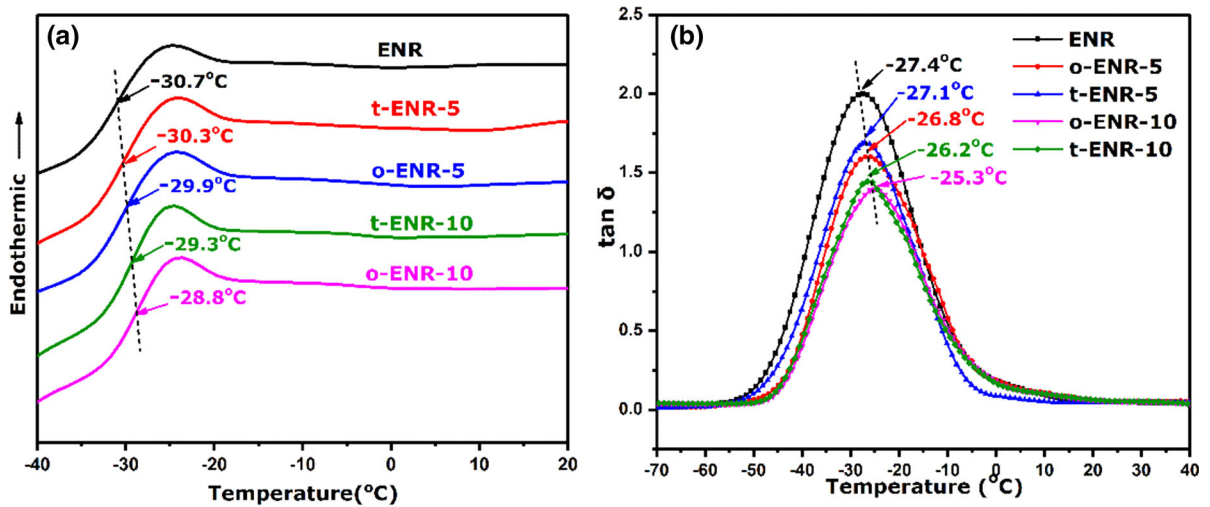
Fig. 5 **a** DSC and **b** DMA curves of neat ENR and ENR/t-CNs nanocomposites
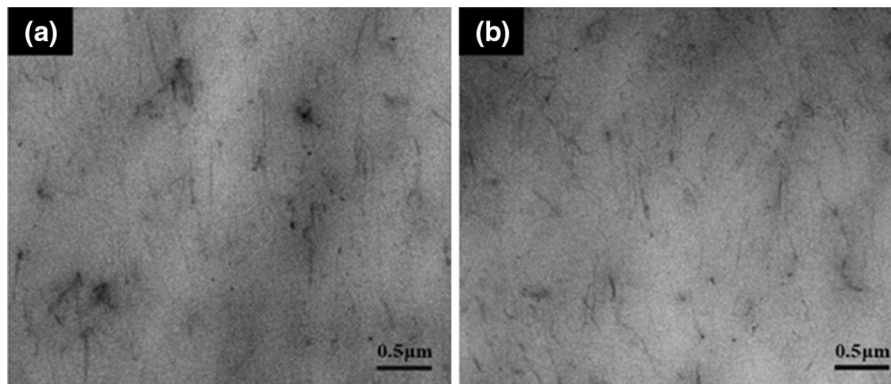

Fig. 6 TEM images of **a** t-ENR-5 nanocomposite and **b** o-ENR-5 nanocomposite

mechanical properties. Therefore, dispersion state of t-CNs in ENR matrix is evaluated by TEM and SEM. As shown in Figs. 6a and 7a, several large aggregates are observed in t-ENR-5 nanocomposites, showing the

relative poor dispersion of t-CNs in t-ENR nanocomposites. However, for o-ENR nanocomposites (as shown in Figs. 6b, 7b), t-CNs are homogeneously dispersed in ENR matrix without any large aggregates,

Fig. 7 SEM images of the cryofractured surfaces of **a** t-ENR-5 nanocomposite and **b** o-ENR-5 nanocomposite
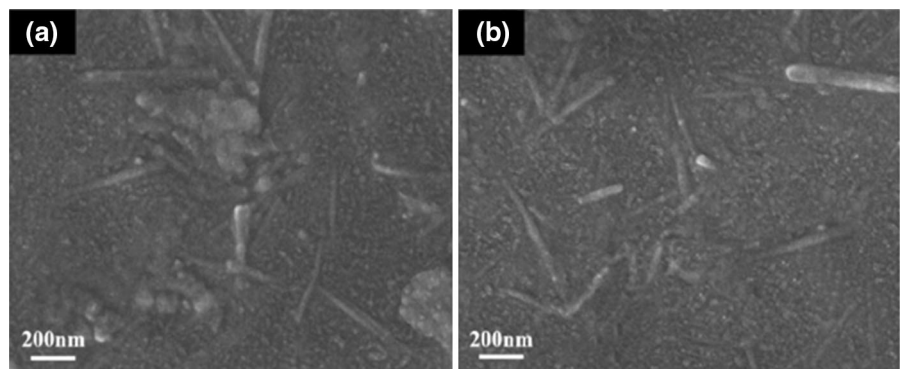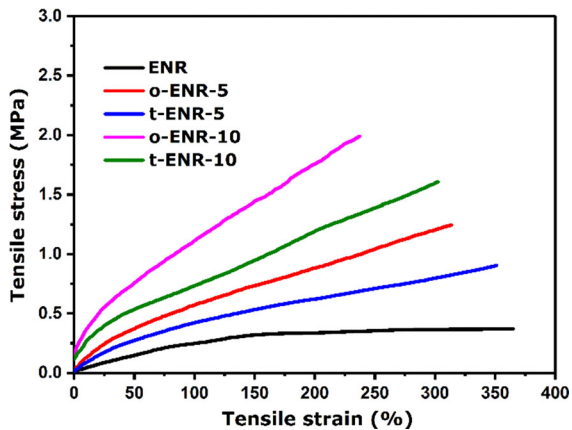
Fig. 8 Representative tensile stress–strain curves of neat ENR and ENR/t-CNs nanocomposites with different t-CNs content

which demonstrate that good compatibility between ENR and t-CNs is achieved. The morphological observation also provide evidence that the interfacial interaction in o-ENR nanocomposites is stronger than that in t-ENR nanocomposites. Such uniform distribution is anticipated to play an important role in improving mechanical properties of the obtained nanocomposites which will be discussed below.

Mechanical properties of ENR/t-CNs nanocomposites

To evaluate the effect of t-CNs as reinforcing phase in ENR matrix, the classical uniaxial tensile tests were performed, as shown in Fig. 8 and Figure S2 (Supporting Information). Tensile properties determined from stress–strain curves are summarized in Table 1. Neat ENR shows a nonlinear stress–strain curve with

relative low strength and high elongation at break. For nanocomposites, the increase in t-CNs content leads to substantial increase in mechanical properties, including ultimate stress and tensile modulus, which indicates the obvious reinforcing efficiency of t-CNs. For example, compared with neat ENR, t-ENR-10 shows 4.5-fold increase in tensile strength and 6.3-fold increase in modulus, while for o-ENR-10, 5.2-fold increase in tensile strength and 9.5-fold increase in modulus are observed.

Compared with t-ENR nanocomposites, more profound reinforcing efficiency is achieved for o-ENR nanocomposites. For example, tensile strength and modulus increased from 1.65 and 3.80 MPa of t-ENR-10 to 1.94 and 5.68 MPa of o-ENR-10, which showed 18 and 50% increasement, respectively. This phenomenon is closely related to the preparation process. For the reinforcing mechanism of elastomer/nanofiller nanocomposites, it is generally believed that there is a glass layer around rubber-filler interface due to the interaction between rubber and filler (Sarkawi et al. 2014). The chain orientation can be easily realized by slipping chains along nanofiller in the glassy layer during stretching (Tang et al. 2012). After the orientation of chains under external stress, the glass layer could act as bridge which facilitates the stress transfer from matrix to nanofiller. The stronger interfacial adhesion is also beneficial for the stress transfer from matrix to nanofiller, which further improves the reinforcing efficiency. In case of o-ENR nanocomposites, the enhanced interfacial interaction could effectively transfer external stress from matrix to t-CNs. Thus, a better reinforcement is achieved. Moreover, the homogeneous dispersion of

Table 1 Mechanical properties of neat ENR and ENR/t-CNs nanocomposites

Samples	Tensile strength (MPa)	Strain to failure (%)	Modulus (MPa)[a]	Stress at 100% strain (MPa)
ENR	0.37 ± 0.03	365 ± 18	0.60 ± 0.08	0.25 ± 0.03
o-ENR-3	0.81 ± 0.05	341 ± 17	1.78 ± 0.15	0.41 ± 0.05
t-ENR-3	0.64 ± 0.04	381 ± 21	0.98 ± 0.12	0.34 ± 0.02
o-ENR-5	1.23 ± 0.11	313 ± 17	2.72 ± 0.17	0.58 ± 0.05
t-ENR-5	0.92 ± 0.04	351 ± 19	1.46 ± 0.16	0.42 ± 0.03
o-ENR-8	1.71 ± 0.13	266 ± 15	3.64 ± 0.22	0.78 ± 0.08
t-ENR-8	1.25 ± 0.13	342 ± 16	2.24 ± 0.20	0.54 ± 0.05
o-ENR-10	1.94 ± 0.16	240 ± 16	5.68 ± 0. 25	1.11 ± 0.12
t-ENR-10	1.65 ± 0.12	303 ± 15	3.80 ± 0.21	0.74 ± 0.04

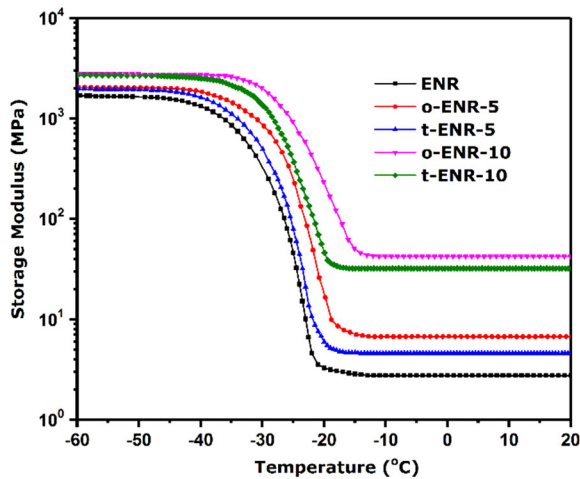[a]Represents experimental data of tensile modulus determined at 5% strain

Fig. 9 Comparison of storage modulus as a function of temperature of neat ENR and ENR/t-CNs nanocomposites

t-CNs in o-ENR nanocomposites also contributes to the improvement of mechanical properties.

In addition, dynamic mechanical analysis (DMA) was also performed to study the reinforcement of the nancomposites in a broad temperature range, as shown in Fig. 9 and Figure S3 (Supporting Information). And storage modulus (E') both at glassy and rubbery state are summarized in Table 2. An obvious improvement in storage modulus is observed by addition of t-CNs into ENR matrix. E' of the nanocomposites are slightly higher than that of neat ENR in glassy state. For example, E' below T_g increased from 1.6 GPa for neat ENR to 2.6 and 2.7 GPa for t-ENR-10 and o-ENR-10, respectively. However, a more dramatic mechanical reinforcement is observed in rubbery state. For example, t-ENR-10 and o-ENR-10 nanocomposites exhibit E' values of 32.1 and 55.6 MPa, respectively, which represent 11.8-fold and 21.8-fold over that of

neat ENR. It should be noted that a larger increase in E' is achieved in o-ENR nanocomposites over the whole temperature range compared with t-ENR nanocomposites. This phenomenon could be understood by considering that the improved dispersion and stronger interfacial interaction in o-ENR nanocomposites, which ensures the efficient stress transfer from matrix to t-CNs. To further estimate the reinforcing efficiency of t-CNs quantitatively, the reinforcement ratios (calculated by using E' at 20 °C for the nanocomposites with respect to neat ENR) are also shown in Table 2. As expected, o-ENR nanocomposites show higher reinforcing efficiency for ENR than t-ENR nanocomposites.

The elastomeric network and interfacial interaction can also be estimated by using the well-known Mooney–Rivlin equation (Bokobza and Erman 2000):

$$\sigma^* = \frac{\sigma}{\lambda - \lambda^{-2}} = 2C_1 + 2C_2\lambda^{-1} \tag{3}$$

where σ is applied stress, λ is extension ratio, and C_1, C_2 are constants that are independent of λ. The plots of reduced stress (σ^*) versus reciprocal of λ are shown in Fig. 10. It can be seen that σ^* of neat ENR is almost constant in the whole extension range, whereas σ^* of the nanocomposites show an abrupt upturn at low λ^{-1}. This upturn is attributed to the finite extensibility of rubber chains bridging neighboring fillers during stretching (Tang et al. 2012). The values of λ^{-1} at which upturn occurs decreased with increasing t-CNs content. This is because increasing t-CNs content will lead to enhanced interfacial interaction, which makes rubber chains easily extend at smaller deformation.

Compared with t-ENR nanocomposites, the absolute values of σ^* increased and the values of λ^{-1} at which upturn occurs decreased consistently of o-ENR

Table 2 Storage modulus (E′) at glassy and rubbery state of neat ENR and ENR/t-CNs nanocomposites

Samples	E' at glassy state (− 50 °C, MPa)	E' at rubbery state (20 °C, MPa)	Reinforcement ratios[a]
ENR	1627 ± 58	2.73 ± 0.2	–
o-ENR-5	2015 ± 72	9.65 ± 0.6	3.53
t-ENR-5	1910 ± 43	4.58 ± 0.4	1.68
o-ENR-8	2251 ± 86	18.45 ± 1.5	6.76
t-ENR-8	2159 ± 102	11.29 ± 0.6	4.14
o-ENR-10	2749 ± 133	59.55 ± 2.4	21.81
t-ENR-10	2645 ± 157	32.12 ± 2.3	11.77

[a]Reinforcement ratios are calculated by using E' at 20 °C for the nanocomposites with respect to neat ENR
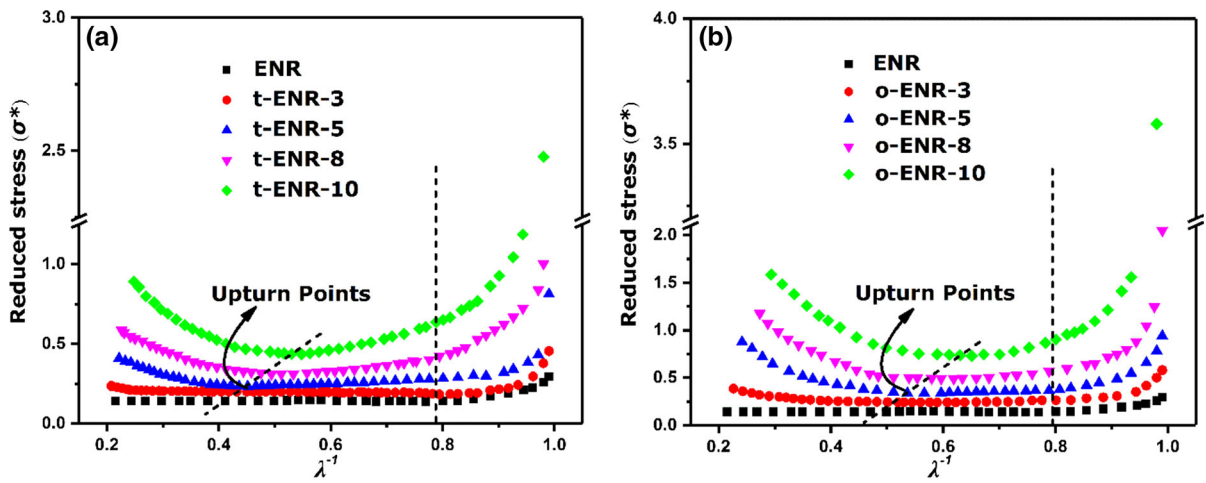
Fig. 10 Reduced stress (σ^*) as a function of λ^{-1} for neat ENR and ENR/t-CNs nanocomposites based on Mooney–Rivlin equation
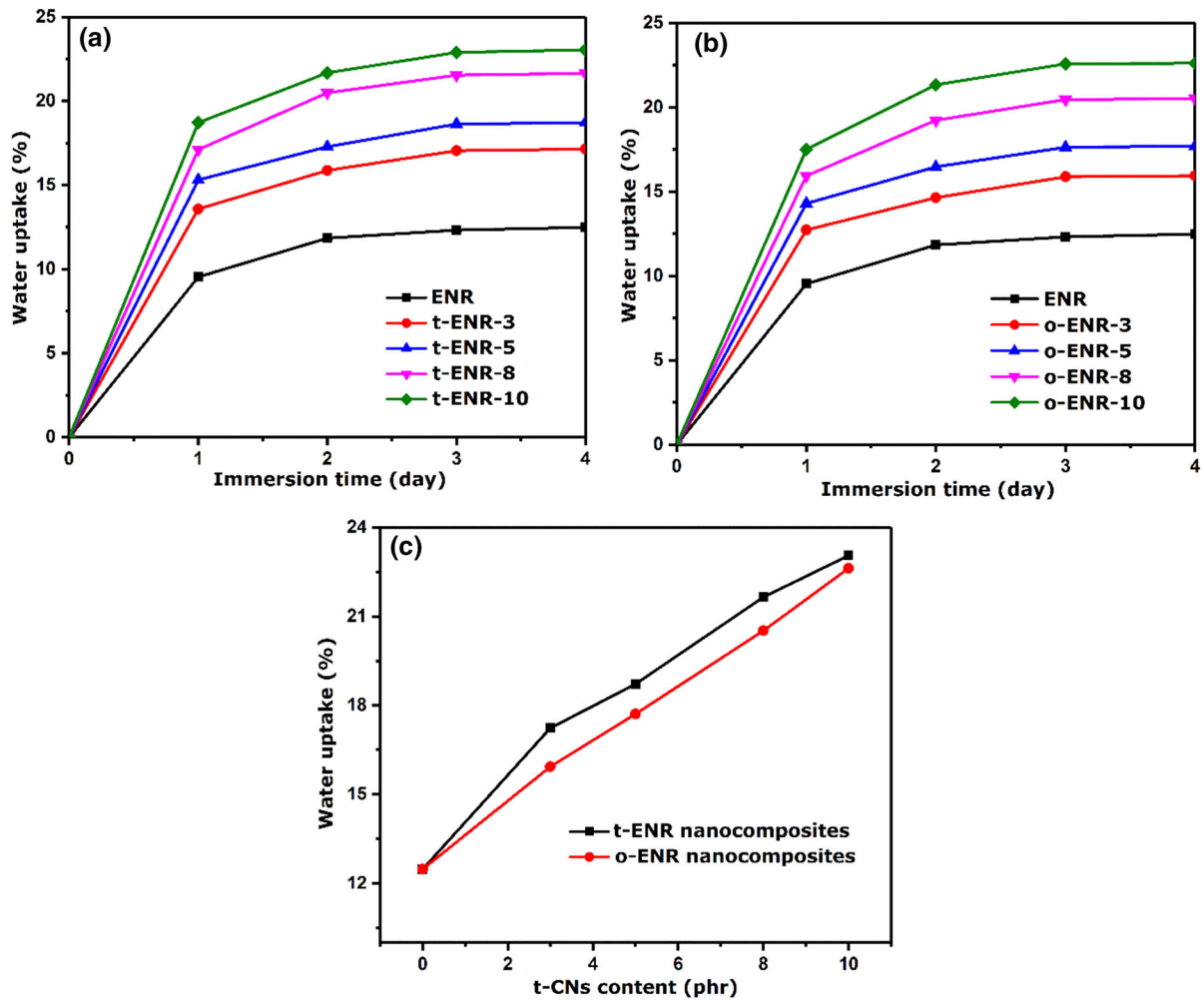

Fig. 11 Water uptake of **a** t-ENR nanocomposites, **b** o-ENR nanocomposites and **c** comparison of water uptake at equilibrium state between t-ENR and o-ENR nanocomposites at various t-CNs content

nanocomposites. Such observations can be explained by the facts that weak interfacial interaction in t-ENR nanocomposites is not strong enough to effectively constrain the mobility of rubber chains, which will lead to the desorption of rubber chains in interface zone. Thus, the finite chain extensibility will appear at larger extension. For o-ENR nanocomposites, improved dispersion and enhanced interfacial adhesion can promote rubber chains to orientate at lower extension by allowing chains to slip along t-CNs surfaces.

Water swelling behavior of ENR/t-CNs nanocomposites

The water-swelling behavior of neat ENR and ENR/t-CNs nanocomposites is also studied, and the results are shown in Fig. 11. As expected, the water uptake at equilibrium state for both nanocomposites increase gradually with increase t-CNs content ascribed to the strong hydrophilic nature of cellulose nanocrystals. In addition, both t-ENR and o-ENR nanocomposites show similar swelling behavior: water uptake go up rapidly in the first day and then increase slowly until reach equilibrium state in 2–3 days. The water uptake at equilibrium state are summarized in Fig. 11c. The weak interfacial interaction results in higher free volume around interface, which is beneficial for water to permeate into matrix (Tang et al. 2012). In this regard, it is well understood that o-ENR nanocomposites show lower equilibrium water uptake compared with t-ENR nanocomposites at same t-CNs content.

Conclusions

In conclusion, we demonstrated a green one-pot method to reinforce ENR by using t-CNs. The results indicated that hydrogen bonds formed in both the nanocomposites and mechanical properties increased with increasing t-CNs content. Moreover, compared with two-step method, one-pot method showed improved dispersion and enhanced interfacial interaction due to the etching effect and possible grafting reaction during one-pot process. This tightly bound the rubber chains to the t-CNs surfaces and was beneficial for stress transfer from the rubber chains to the t-CNs. As result, compared with two-step method, 20, 50 and

85% increase in tensile strength, tensile modulus and rubbery storage modulus were achieved for one-pot method at 10 phr t-CNs. In addition, one-pot method showed decreased water uptake due to the enhanced interfacial interaction, which depressed water permeation because of lower free volume at interface. We envisioned that this work would contribute new method to prepare high performance diene based rubber/CNs nanocomposites.

References

Bitinis N, Verdejo R, Bras J et al (2013) Poly(lactic acid)/natural rubber/cellulose nanocrystal bionanocomposites part I: Processing and morphology. Carbohydr Polym 96:611–620

Bokobza L, Erman B (2000) A theoretical and experimental study of filler effect on stress-deformation-segmental orientation relations for poly(-dimethylsiloxane) networks. Macromolecules 33:8858–8864

Cao XD, Habibi Y, Lucia LA (2009) One-pot polymerization, surface grafting, and processing of waterborne polyurethane-cellulose nanocrystal nanocomposites. J Mater Chem 19:7137–7145

Cao XD, Xu CH, Liu YH et al (2013) Preparation and properties of carboxylated styrene-butadiene rubber/cellulose anocrystals composites. Carbohyd Polym 92:69–76

Cao LM, Fu XF, Xu CH et al (2017a) High-performance natural rubber nanocomposites with marine biomass (tunicate cellulose). Cellulose 24:2849–2860

Cao LM, Yuan DS, Xu CH et al (2017b) Biobased, self-healable, high strength rubber with tunicate cellulose nanocrystals. Nanoscale 9:15696–15706

Chen YK, Zhang YB, Xu CH et al (2015) Cellulose nanocrystals reinforced foamed nitrile rubber nanocomposites. Carbohyd Polym 130:149–154

Chen YK, Wang YH, Xu CH et al (2016) New approach to fabricate novel fluorosilicone thermoplastic vulcanizate with bicrosslinked silicone rubber-core/fluororubbershell particles dispersed in poly(vinylidene fluoride): structure and property. Ind Eng Chem Res 55:1701–1709

Chen YK, Huang XH, Gong Z et al (2017) Fabrication of high performance magnetic rubber from NBR and Fe_3O_4 via in situ compatibilization with zinc dimethacrylate. Ind Eng Chem Res 56:183–190

Chen YK, Wang WT, Yuan DS et al (2018) Bio-based PLA/NR-PMMA/NR ternary thermoplastic vulcanizates with

balanced stiffness and toughness: "Soft–Hard" core–shell continuous rubber phase, in situ compatibilization, and properties. ACS Sustain Chem Eng 6:6488–6496

Favier V, Chanzy H, Cavaille JY (1995) Polymer nanocomposites reinforced by cellulose whiskers. Macromolecules 28:6365–6367

Fortunati E, Luzi F, Puglia D et al (2015) Processing of PLA nanocomposites with cellulose nanocrystals extracted from Posidonia oceanica waste: innovative reuse of coastal plant. Ind Crop Prod 67:439–447

Fox J, Wie JJ, Greenland BW et al (2012) High-Strength, healable, supramolecular polymer nanocomposites. J Am Chem Soc 134:5362–5368

Fu LH, Wu FD, Xu CH et al (2018) Anisotropic shape memory behaviors of polylactic acid/citric acid-bentonite composite with a gradient filler concentration in thickness direction. Ind Eng Chem Res 57:6265–6274

George N, Bipinbal PK, Bhadran B et al (2017) Segregated network formation of multiwalled carbon nanotubes in natural rubber through surfactant assisted latex compounding: a novel technique for multifunctional properties. Polymer 112:264–277

Goetz L, Foston M, Mathew AP et al (2010) Poly(methyl vinyl ether-co-maleic acid)–polyethylene glycol nanocomposites cross-linked in situ with cellulose nanowhiskers. Biomacromol 11:660–2666

Ha QX, Wu YP, Wang YQ et al (2008) Enhanced interfacial interaction of rubber/clay nanocomposites by a novel two-step method. Compos Sci Technol 68:1050–1056

Kanoth BP, Claudino M, Johansson M et al (2015) Biocomposites from natural rubber: synergistic effects of functionalized cellulose nanocrystals as both reinforcing and crosslinking agents via free-radical thiol-ene chemistry. ACS Appl Mater Interfaces 7:16303–16310

Lin N, Dufresne A (2013) Physical and/or chemical compatibilization of extruded cellulose nanocrystal reinforced polystyrene nanocomposites. Macromolecules 46:5570–5583

Lin N, Huang J, Dufresne A (2012) Preparation, properties and applications of polysaccharide nanocrystals in advance functional nanomaterials: a review. Nanoscale 4:3274–3294

Liu MX, Peng Q, Luo BH, Zhou CR (2015a) The improvement of mechanical performance and water-response of carboxylated SBR by chitin nanocrystals. Eur Polym J 68:190–206

Liu X, Kuang WY, Guo BC (2015b) Preparation of rubber/grapheme oxide composites with in situ interfacial design. Polymer 56:553–562

Liu XH, Lu CH, Wu XD et al (2017) Self-healing strain sensors based on nanostructured supramolecular conductive elastomers. J Mater Chem A 5:9824–9832

Mariano M, Kissi NE, Dufresne A (2016) Cellulose nanocrystal reinforced oxidized natural rubber nanocomposites. Carbohyd Polym 137:174–183

Miao CW, Haman W (2016) In-situ polymerized cellulose nanocrystals (CNC)-poly(l-lactide) (PLLA) nanomaterials and applications in nanocomposite processing. Carbohyd Polym 153:549–558

Moon RJ, Martini A, Nairn J et al (2011) Cellulose nanomaterials review: structure, properties and nanocomposites. Chem Soc Rev 40:3941–3994

Oksman K, Aitomaki Y, Mathew A et al (2016) Review of the recent development in cellulose nanocomposites processing. Compos Part A-Appl Sci 83:2–18

Pei A, Malho JM, Ruokolainen J et al (2011) Strong nanocomposite reinforcement effects in polyurethane elastomer with low volume fraction of cellulose nanocrystals. Macromolecules 44:4422–4427

Sacui IA, Nieruwendaal RC, Burnett DJ et al (2014) Comparison of the properties of cellulose nanocrystals and cellulose nanofibrils isolated from bacteria, tunicate, and wood processed using acid, enzymatic, mechanical, and oxidative methods. ACS Appl Mater Interfaces 6:6127–6138

Saralegi A, Gonzalez ML, Valea A et al (2014) The role of cellulose nanocrystals in the improvement of the shape-memory properties of castor oil-based segmented thermoplastic polyurethanes. Compos Sci Technol 92:27–33

Sarkawi SS, Dierkes WK, Noordermeer JWM (2014) Elucidation of filler-to-filler and filler-to-rubber interactions in silica-reinforced natural rubber by TEM network visualization. Eur Polym J 54:118–127

Scafaro R, Botta L, Lopresti F et al (2017) Polysaccharide nanocrystals as fillers for PLA based nanocomposites. Cellulose 24:447–478

Song T, Tanpichai S, Oksman K (2016) Cross-linked polyvinyl alcohol (PVA) foams reinforced with cellulose nanocrystals (CNCs). Cellulose 23:1925–1938

Spinella S, Re GL, Liu B et al (2015) Polylactide/cellulose nanocrystal nanocomposites: efficient routes for nanofiber modification and effects of nanofiber chemistry on PLA reinforcement. Polymer 65:9–17

Tang ZH, Wu XH, Guo BC et al (2012) Preparation of butadiene–styrene–vinyl pyridine rubber–graphene oxide hybrids through co-coagulation process and in situ interface tailoring. J Mater Chem 22:7492–7501

Tian M, Zhen XC, Wang ZF et al (2016) Bioderived rubber-cellulose nanocrystal composites with tunable water-responsive adaptive mechanical behavior. ACS Appl Mater Interfaces 9:6482–6487

Wolff S, Wang MJ, Tan EH (1993) Filler-elastomer interactions. Part VII. Study on bound rubber. Rubber Chem Technol 66:163–177

Xu TW, Jia ZX, Luo YF et al (2015) Interfacial interaction between the epoxidized natural rubber and silica in natural rubber/silica composites. Appl Surf Sci 328:306–313

Xu CH, Cao LM, Lin BF et al (2016) Design of self-healing supramolecular rubbers by introducing ionic cross-links into natural rubber via a controlled vulcanization. ACS Appl Mater Interfaces 8:17728–17737

Xu CH, Cao LM, Huang XH et al (2017) Self-healing natural rubber with tailorable mechanical properties based on ionic supramolecular hybrid network. ACS Appl Mater Interfaces 9:29363–29373

Xu CH, Zhan W, Tang XZ et al (2018) Self-healing chitosan/vanillin hydrogels based on Schiff-base bond/hydrogen bond hybrid linkages. Polym Test 66:155–163

Yan HQ, Chen XQ, Song HW et al (2017) Synthesis of bacterial cellulose and bacterial cellulose nanocrystals for their

applications in the stabilization of olive oil pickering emulsion. Food Hydrocoll 72:127–135

Ye YS, Zeng HX, Wu J et al (2016) Biocompatible reduced graphene oxide sheets with superior water dispersibility stabilized by cellulose nanocrystals and their polyethylene oxide composites. Green Chem 18:1674–1683

Yu HP, Zeng ZQ, Lu G et al (2008) Processing characteristics and thermal stabilities of gel and sol of epoxidized natural rubber. Eur Polym J 44:453–464

Yu J, Wang CP, Wang JF et al (2016) In situ development of self-reinforced cellulose nanocrystals based thermoplastic elastomers by atom transfer radical polymerization. Carbohyd Polym 141:143–150

Zhang SD, Liu F, Peng HQ et al (2015) Preparation of novel c–6 position carboxyl corn starch by a green method and its application in flame retardance of epoxy resin. Ind Eng Chem Res 54:11944–11952

Zhao YD, Li JB (2014) Excellent chemical and material cellulose from tunicates: diversity in cellulose production yield and chemical and morphological structures from different tunicate species. Cellulose 21:3427–3441

Zhao YD, Zhang YJ, Lindstrom ME et al (2015) Tunicate cellulose nanocrystals: preparation, neat films and nanocomposite films with glucomannans. Carbohyd Polym 117:286–296